Novel Use of Differential Image Velocity Invariants to Categorize Ciliary Motion Defects

Shannon Quinn*, Richard Francis†§, Cecilia Lo†§ and Chakra Chennubhotla‡§
*Joint Carnegie Mellon University–University of Pittsburgh Ph.D. Program in Computational Biology,
†Department of Developmental Biology, ‡Department of Computational and Systems Biology,
§University of Pittsburgh School of Medicine, Pittsburgh, PA 15260

***Abstract*—Primary ciliary dyskinesia (PCD) is a disorder characterized by sinopulmonary disease arising from ciliary motion defects in respiratory epithelia. An essential first step in the diagnostic evaluation of PCD is the use of high-speed videomicroscopy to analyze ciliary beat patterns in nasal epithelia biopsies. This includes a quantitative assessment of ciliary beat frequency (CBF, where CBF of < 11 Hz is referred to further diagnosis), followed by a visual examination of ciliary beat patterns to detect the presence of dyskinetic motions, such as *stiff*, *incomplete*, *wavy* and others. Both procedures lack standardized protocols, hence CBF is often counted manually by observing the ciliary image frames in slow motion, while a manual examination of beat patterns is subjective, cumbersome, and error-prone. We are building automated image analysis methods to address this problem. To this end, we report the use of image velocities for measuring CBF and demonstrate the effectiveness of the differential image velocity invariants, *curl* and *deformation*, in deconvolving the various motion defects.**

I. Introduction

Primary ciliary dyskinesia (PCD) [1], [2] is a genetically heterogeneous disorder characterized by sino-pulmonary disease, laterality defects (abnormal placement of organs in the body), and male infertility. PCD is autosomal recessive [3], [4] with an incidence rate of around 1:15000 in the Caucasian population. Defects in the structure and function of motile cilia, the hairlike projections from cell surfaces, are associated with a range of human diseases, including PCD, congenital heart disease [5], [6], [7], polycystic liver and kidney disease [8], and many others [9].

For diagnosing PCD it is a common practice on the clinical side to assess for the effectiveness of mucociliary clearance, and test for low nasal nitric oxide (nNO) levels [10], [11], however this is unreliable with young children, and low nNO is also seen in other pulmonary diseases. Transmission electron microscopy (TEM) of ciliated epithelia can be used to inspect defects in the ciliary ultrastructure and determine ciliary orientation within cells [12], [13], however some of the ciliary structures are difficult to detect due to low contrast [14]. High-resolution immunofluorescence is extremely useful and can identify several subtle ultrastructural defects [15], but it requires the cells to be fixed, making live observations impossible. High-speed videomicroscopy has become one of the more popular methods [16] for its simplicity and ability to capture specific beat patterns that correspond to different ultrastructural defects, and in practice it has become an essential first step in the diagnostic evaluation for PCD [17]. This includes a (i) quantitative assessment of ciliary beat frequency (CBF) and (ii) qualitative assessment of ciliary beat patterns for abnormalities [18]. However, both these procedures suffer from lack of a standardized protocol.

Ciliary oscillations are often counted manually by observing the image frames in slow motion. This has also made such diagnostic assessments cumbersome, expensive, and error-prone, and impossible to execute on a large-scale, as comparing findings procured manually from different clinical centers is difficult. In addition, for many patients PCD is diagnosed much later in life when permanent lung damage has already occurred [19]. Thus, early and accurate diagnosis using quantitative, automated methods can have a significant impact on both short-term and long-term morbidity, as lung function can be maintained, unnecessary ear, nose and throat surgery can be prevented and lung transplants can be avoided [20].

We address the need for a standardized and accurate diagnosis of PCD with automated videomicroscopy analysis methods. In particular, we report here our preliminary work on using image velocities for measuring ciliary beat frequency and differential image velocity invariants, curl and deformation, for deconvolving the various motion defects. We approach the task of automating ciliary beat pattern analysis as a problem in dynamic texture analysis and synthesis [21]. Dynamic textures–such as motion sequences of fire, smoke, water, foliage or flowers in the wind, and crowds of people waving–commonly exhibit some form of temporal regularity. Ciliary beat patterns also constitute dynamic textures: the sweeping motion consists of forward and backward stroke of the cilia executed rhythmically across the surface of the respiratory epithelium. Early on, Julesz (1962) observed that there is a correlation between statistical and perceptual similarity of (dynamic) textures [22]. Following this key observation, we hypothesize that the perceptual correlates, e.g. wavy, stiff etc., derived from a visual inspection of ciliary motion videos can be attributed to the fluctuations of stochastically-driven harmonic oscillators, whose properties can be captured by image velocity differentials.

II. Data

Ciliated nasal epithelium was collected from volunteer patients using curettage. The volunteers had been diagnosed with cogenital heart disease (CHD) and heterotaxy, as a consequence of which the patients often develop respiratory

issues. Thus, CHD associated with heterotaxy is hypothesized to share a common etiology with PCD [23]. The ciliary nasal tissue was suspended in small L-15 medium for videomicroscopy using a Leica inverted microscope (DMIRE2) with a 100X oil objective under DIC optics. Several dozen digital movies of cilia from a handful of patients exhibiting normal and abnormal ciliary motion were recorded at 200 Hz at room temperature using a Phantom v4.2 camera. These digital recordings were then evaluated by a blinded expert panel [23] in order to determine motion categories (stiff, wavy, etc). All videos are in AVI format, are typically at least half a minute in length, and are grouped according to manual expert labeling. Two consecutive example frames from one video in the data set can be seen in Fig 1. All videos are taken from this top-down perspective, allowing us to analyze the cilia that are effectively lying flat within the camera's two-dimensional plane of focus.

III. Methods

A. Estimate image velocities

We invoke the standard brightness constancy assumption

$$I(x, y, t) = I(x + u\delta t, y + v\delta t, t + \delta t), \tag{1}$$

which states that the image intensity (or a filtered version of it) I at pixel location (x, y) at time t is preserved locally for small changes $(u\delta t, v\delta t)$ observed in space in a small time interval δt. Here (u, v) constitute the horizontal and vertical image velocites, also called the optical flow, at (x, y). A gradient constraint follows from the brightness constancy assumption to combine spatial derivatives (I_x, I_y) and temporal derivative I_t with optical flow [24],

$$I_x u + I_y v + I_t = 0. \tag{2}$$

The gradient constraints pooled over a small neighborhood around pixel (x, y) form an overdetermined system of linear equations from which the optical flow is derived. We use a variation of the classical optical flow algorithm suggested by Black and co-workers [25] that incorporates a non-local smoothness terms to integrate information over large spatial neighborhoods.

Results: Fig. 1 shows two consecutive frames from an abnormal ciliary motion sequence (panels A and B) and the estimated optical flow in a vector form (C) and a color coded diagram with flow amplitude $a = \sqrt{(u^2 + v^2)}$ computed at each pixel (D). It is possible that that the brightness constancy assumption may not truly hold, as ciliary motions can cause occlusion or cilia from overlapping cells might occlude one another. We plan to investigate this issue in more detail in the future.

B. Estimate CBF from motion amplitude waveforms

Before computing CBF, background pixels which are near-stationary, i.e. they exhibit small motion amplitudes over the entire course of the video, are identified by applying a suitable threshold on the variance of the amplitude distributions at each pixel. The threshold is data-driven and operator independent.

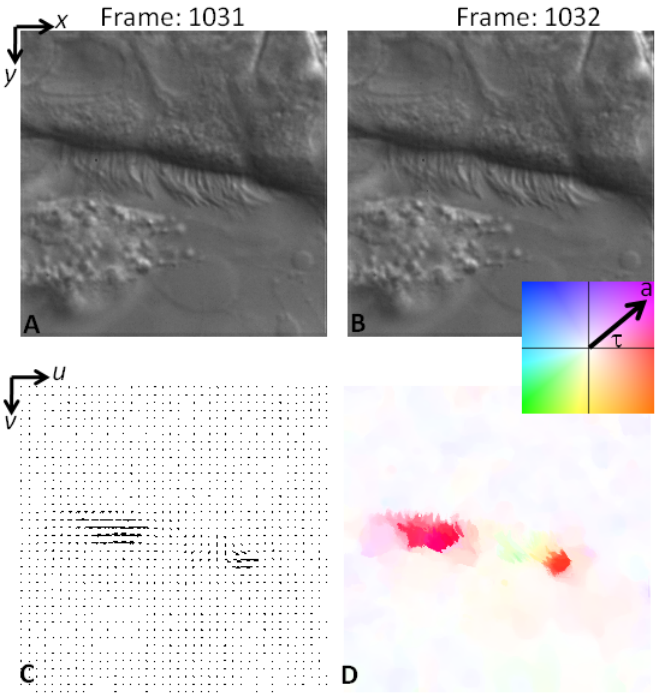

Fig. 1. (A,B) Two consecutive frames of a ciliary motion video undergoing abnormal motion. Optical flow computed with algorithm in [25] is shown as a (C) vector field and (D) color coded with amplitude $a = \sqrt{u^2 + v^2}$ and angle $\tau = \arctan(u, v)$.

After identifying pixels demonstrating motion between frames (Fig 1), the amplitude waveform at each pixel is analyzed with a discrete fourier transform and the peaks of the power spectrum are used to identify the dominant ciliary beat frequency automatically.

Results: In Fig. 2 we show the results from estimating CBF for the video in Fig. 1. Any frequency less than 3Hz is suppressed and is shown in white along with the background pixels. There are two dominant frequences: 6.7Hz and 13.3Hz clearly visible in the motion video. The pixels on the cell wall are mostly in blue indicating very little motion and some of the medium surrounding the tips of the cilia is also in blue. Optical flow measurements have been used before by Vozzi et al [26] in computing CBF, however the flow fields are estimated at a sparse set of pixels. Instead, we are computing a dense optical flow field and providing a complete distribution of the ciliary beat frequencies for a more quantitative analysis. It is worth noting that there is much debate in the community on the use of CBF in diagnosing PCD [17], [18] and it is generally agreed that beat pattern analysis has more diagnostic value. Next, we present a novel approach to beat pattern analysis.

C. Find differential image velocity invariants

Differential image velocity invariants [27] have been used before to characterize and classify dynamic textures. We use the well-known result from Koenderink and Van Doorn [28], [29] showing how to decompose optical flow fields into first-

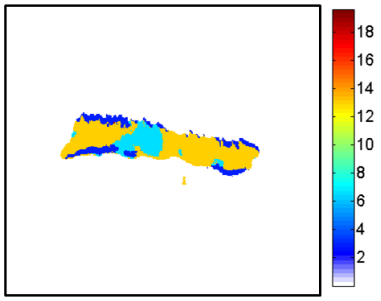

Fig. 2. CBF is automatically estimated from the peaks of the power spectrum of the flow amplitude signal. CBF results here are for the video shown in Fig. 1. CBF values are color coded at each pixel and the color bar indicates CBF in Hz (the video was captured at 200Hz). The background pixels are all shown in white color.

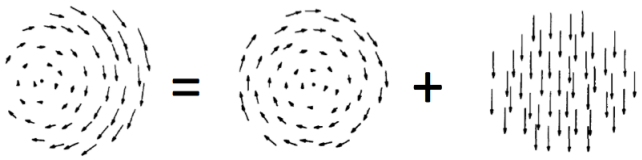

Fig. 3. Hypothetical motion at the tips of the cilia decomposed into two simpler waveforms: circular plus downward translation. Curl, divergence, and deformation can be derived from optical flow. The amount of curl in the flow field in the left hand side above is exactly the same as that in the first operand, but is zero for translation-only motion. These first-order differentials are invariant to image rotation and translation, thus providing a quantitative basis for discriminating ciliary motions.

order differential components:

$$\begin{aligned} \text{curl } \mathbf{u} &= -(u_y - v_x), \\ \text{div } \mathbf{u} &= (u_x + v_y), \\ (\text{def } \mathbf{u}) \cos 2\mu &= (u_x - v_y), \\ (\text{def } \mathbf{u}) \sin 2\mu &= (u_y + v_x), \end{aligned} \tag{3}$$

where the subscripted horizontal and vertical image velocities: (u_x, u_y) and (v_x, v_y) correspond to spatial flow derivatives. Curl, divergence (div) and deformation (def) capture spatial distortions in the form of rotation, expansion (or scaling) and biaxial shear, respectively. We hypothesize that even ciliary motions can be approximated by these image velocity gradients. As shown in Fig. 3, it is conceivable the beat pattern at the tips of the cilia in the multi-ciliated epithelia can be represented as a vector flow of two simpler waveforms: circular plus downward translation. Curl, divergence, and deformation are particularly convenient properties of the video, as they are rotation and translation invariant.

Results: We run a first-derivative of a Gaussian filter (with $\sigma = 1$) to compute the spatial derivatives of the optical flow in the x and y directions and ignore information from the background pixels identified earlier.

D. Use curl and deformation magnitude as motion signatures

We study the feasibility of distinguishing abnormal ciliary waveforms seen in heterotaxy patients, described as wavy or stiff, from normal ciliary motion seen in control individuals. Our goal is to compute the differential invariants for all

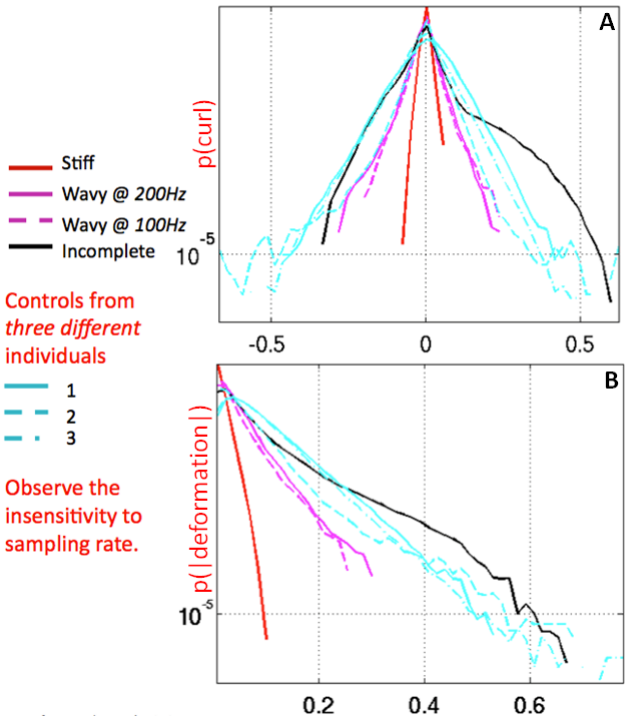

Fig. 4. (frequency is plotted as a histogram for each property) We see that there is good separation between the motion categories using curl and deformation as features. Divergence is not shown, as its histogram shows overlap between the various motion patterns, making its use as a discriminative property negligible.

the motion frames and study the probability distributions summarized over all the pixels. Having removed the background pixels, we hope for the histograms to reveal features characteristic to the motion type.

Results: We decompose labeled videos of different motion types–normal, wavy, and so on–and calculate the CBFs of the videos along with the image velocity invariants. The histograms in Fig. 4 show the probability distributions for curl (panel A) and deformation magnitude (B), for motion categories of stiff, wavy and incomplete, along with the controls from three different inviduals. The most distinguishing feature is the separation in the tails of the distributions. Stiff and incomplete motions form the extrema of the distributions and are easily separable. However, the wavy and control motions overlap for a significant portion of the allowable curl and deformation magnitudes. For robustness, we varied the sampling rate to observe that the curl and deformation magnitude histograms are insensitive. We also observed that divergence is not a good discrimant of the motion categories (data not shown). The separation in the histograms is being caused by the tails of the respective distributions, as a consequence we expect a significant amount of motion data has to be collected and analyzed before the tails become sufficiently discriminative.

IV. Conclusions and Future Work

We invoked brightness constancy assumption to estimate image velocities from high resolution high-speed video mi-

croscopy of human airway ciliary motions. CBF was robustly estimated from the periodic motion amplitude signal, thus allowing easy automation of determining CBF. We characterized ciliary motions patterns using differential image velocity invariants, curl and deformation magnitude. These quantities provided robust signatures for separating ciliary motion classes. Therefore, we believe image velocity invariants can be effectively used to deconvolve the complexities of human airway ciliary motion, allowing not only the automation of CBF estimation, but also an objective classification of different types of abnormal ciliary motion based on quantitative parameters. Using this novel approach, we have been able to distinguish abnormal ciliary motion previously described as wavy, stiff, or incomplete stroke from patients with heterotaxy vs. normal ciliary motion of healthy controls.

In the future, we plan to incorporate this strategy into a diagnostic toolbox, a complete system that can be utilized by clinicians for rapid and quantitative diagnosis of PCD. Furthermore, we plan to expand upon the initial foundation of using curl and divergence and will introduce low-dimensional generative models of ciliary motion and test their effectiveness on videos sampled at low-resolutions.

REFERENCES

[1] B. A. Afzelius, "A human syndrome caused by immote cilia," *Science*, vol. 93, pp. 317–319, 1976.

[2] R. Eliasson, B. Mossberg, P. Camner, and B. A. Afzelius, "The immotile-cilia syndrome: A congenital ciliary abnormality as an etiologic factor in chronic airway infections and male sterility," *New England Journal of Medicine*, vol. 297, pp. 1–6, 1977.

[3] V. A. McKusick, *Mendelian inheritance in man*, 10th ed. Baltimore: Johns Hopkins University Press, 1992.

[4] D. Narayan, S. N. Krishnan, M. Upender, T. S. Ravikumar, M. J. Mahoney, T. F. D. Jr, A. S. Teebi, and G. G. Haddad, "Unusual inheritance of primary ciliary dyskinesia," *Journal of Medical Genetics*, vol. 31, pp. 493–496, 1994.

[5] N. Katsanis, "The oligogenic properties of Bardet-Biedl syndrome," *Human Molecular Genetics*, vol. 13, no. Review Issue 1, p. R65, 2004.

[6] H. Kulaga, C. Leitch, E. Eichers, J. Badano, A. Lesemann, B. Hoskins, J. Lupski, P. Beales, R. Reed, and N. Katsanis, "Loss of BBS proteins causes anosmia in humans and defects in olfactory cilia structure and function in the mouse," *Nature Genetics*, vol. 36, no. 9, pp. 994–998, 2004.

[7] S. Tan, J. Rosenthal, X. Zhao, R. Francis, B. Chatterjee, S. Sabol, K. Linask, L. Bracero, P. Connelly, M. Daniels *et al.*, "Heterotaxy and complex structural heart defects in a mutant mouse model of primary ciliary dyskinesia," *Journal of Clinical Investigation*, vol. 117, no. 12, pp. 3742–3752, 2007.

[8] B. Yoder, X. Hou, and L. Guay-Woodford, "The polycystic kidney disease proteins, polycystin-1, polycystin-2, polaris, and cystin, are co-localized in renal cilia," *Journal of the American Society of Nephrology*, vol. 13, no. 10, p. 2508, 2002.

[9] J. Badano, N. Mitsuma, P. Beales, and N. Katsanis, "The ciliopathies: an emerging class of human genetic disorders," *Annual Review of Genomics and Human Genetics*, vol. 7, no. 1, p. 125, 2006.

[10] I. Narang, R. Ersu, N. Wilson, and A. Bush, "Nitric oxide in chronic airway inflammation in children: diagnostic use and pathophysiological significance," *Thorax*, vol. 57, no. 7, p. 586, 2002.

[11] N. Nakhleh, M. Swisher, R. Francis, R. Giese, B. Chatterjee, P. Connelly, I. Sami, K. Kuehl, K. Olivier, R. Jonas *et al.*, "Low Nasal Nitric Oxide and Ciliary Dysmotility in Patients with Congenital Heart Disease and Heterotaxy: The Challenge of Defining a Ciliopathy." *American Journal of Respiratory and Critical Care Medicine*, vol. 179, no. 1 MeetingAbstracts, p. A2213, 2009.

[12] A. Bush, P. Cole, M. Hariri, I. Mackay, G. Phillips, C. O'Callaghan, R. Wilson, and J. Warner, "Primary ciliary dyskinesia: diagnosis and standards of care," *European Respiratory Journal*, vol. 12, no. 4, p. 982, 1998.

[13] C. Rayner, A. Rutman, A. Dewar, M. Greenstone, P. Cole, and R. Wilson, "Ciliary disorientation alone as a cause of primary ciliary dyskinesia syndrome," *American Journal of Respiratory and Critical Care Medicine*, vol. 153, no. 3, p. 1123, 1996.

[14] E. Escudier, M. Couprie, B. Duriez, F. Roudot-Thoraval, M. Millepied, V. Pruliere-Escabasse, L. Labatte, and A. Coste, "Computer-assisted analysis helps detect inner dynein arm abnormalities," *American Journal of Respiratory and Critical Care Medicine*, vol. 166, no. 9, p. 1257, 2002.

[15] P. Noone, M. Leigh, A. Sannuti, S. Minnix, J. Carson, M. Hazucha, M. Zariwala, and M. Knowles, "Primary ciliary dyskinesia: diagnostic and phenotypic features," *American Journal of Respiratory and Critical Care Medicine*, vol. 169, no. 4, p. 459, 2004.

[16] M. Zariwala, M. Knowles, and H. Omran, "Genetic defects in ciliary structure and function," *Physiology*, vol. 69, no. 1, p. 423, 2007.

[17] M. Chilvers, A. Rutman, and C. O'Callaghan, "Ciliary beat pattern is associated with specific ultrastructural defects in primary ciliary dyskinesia," *Journal of Allergy and Clinical Immunology*, vol. 112, no. 3, pp. 518–524, 2003.

[18] M. Chilvers and C. O'Callaghan, "Analysis of ciliary beat pattern and beat frequency using digital high speed imaging: comparison with the photomultiplier and photodiode methods," *British Medical Journal*, vol. 55, no. 4, p. 314, 2000.

[19] M. Swisher, R. Jonas, X. Tian, E. Lee, C. Lo, and L. Leatherbury, "Increased postoperative and respiratory complications in patients with congenital heart disease associated with heterotaxy," *The Journal of Thoracic and Cardiovascular Surgery*, 2010.

[20] A. Ellerman and H. Bisgaard, "Longitudinal study of lung function in a cohort of primary ciliary dyskinesia," *European Respiratory Journal*, vol. 10, no. 10, pp. 2376–2379, 1997.

[21] G. Doretto, A. Chiuso, Y. Wu, and S. Soatto, "Dynamic textures," *International Journal of Computer Vision*, vol. 51, no. 2, pp. 91–109, 2003.

[22] B. Julesz, "Visual pattern discrimination," *IRE Transactions on Information Theory*, vol. 8, no. 2, pp. 84–92, 1962.

[23] N. Nakhleh, R. Francis, R. Giese, X. Tian, M. Swisher, S. Kureshi, B. Chatterjee, P. Connelly, N. Kravitz, I. Sami, K. Kuehl, K. Burns, H. Omran, K. Olivier, M. Leigh, M. Knowles, R. Jonas, L. Leatherbury, and C. W. Lo, "Ciliary dysfunction in heterotaxy patients with congenital heart disease: the challenge of defining a ciliopathy," Under Review.

[24] B. Horn and B. Schunck, "Determining optical flow," *Artificial Intelligence*, vol. 16, pp. 185–203.

[25] D. Sun, S. Roth, and M. J. Black, "Secrets of optical flow estimation and their prinicples," in *IEEE Conference on Computer Vision and Pattern Recognition, CVPR*, 2010.

[26] G. Mantovani, M. Pifferi, and G. Vozzi, "Automated software for analysis of ciliary beat frequency and metachronal wave orientation in primary ciliary dyskinesia," *Eur Arch Otorhinolaryngol*, vol. 267, pp. 897–902, 2010.

[27] S. Fazekas, T. Amiaz, D. Chetverikov, and N. Kiryati, "Dynamic texture detection based on motion analysis," *International Journal of Computer Vision*, vol. 82, no. 1, pp. 48–63, 2009.

[28] J. Koenderink and A. J. van Doorn, "Invariant properties of the motion parallax field due to the movement of rigid bodies relative to an observer," *Optica Acta*, vol. 22, no. 9, pp. 773–791, 1975.

[29] ——, "How an amulant observer can construct a model of the envirnoment from the geometrical structure of the visual flow," *Kybernetik*, pp. 224–247, 1978.